AGU
ADVANCING
EARTH AND
SPACE SCIENCES

Geophysical Research Letters®

Key Points:

- Warm-phase invigoration of clouds by air pollution requires supersaturations well in excess of 1% in relatively unpolluted cloudy updrafts
- Observed warm-phase clouds convecting over the Amazon have typical supersaturations around 0.2%
- Observed supersaturations are too low for air pollution to have any practical impact on updraft speeds via warm-phase invigoration

Air Pollution Unable to Intensify Storms via Warm-Phase Invigoration

David M. Romps[1,2] ⓘ, Katie Latimer[3], Qindan Zhu[1] ⓘ, Tina Jurkat-Witschas[4] ⓘ, Christoph Mahnke[5] ⓘ, Thara Prabhakaran[6], Ralf Weigel[7], and Manfred Wendisch[8] ⓘ

[1]Department of Earth and Planetary Science, University of California, Berkeley, CA, USA, [2]Climate and Ecosystem Sciences Division, Lawrence Berkeley National Laboratory, Berkeley, CA, USA, [3]Oakland, CA, USA, [4]Institut für Physik der Atmosphäre, Deutsches Zentrum für Luft- und Raumfahrt (DLR), Oberpfaffenhofen, Germany, [5]Institute of Energy and Climate Research, IEK8, Forschungszentrum Jülich GmbH, Jülich, Germany, [6]Indian Institute of Tropical Meteorology, Pune, India, [7]Institute for Physics of the Atmosphere, Johannes Gutenberg University, Mainz, Germany, [8]Faculty of Physics and Earth Sciences, Leipzig Institute for Meteorology, Leipzig University, Leipzig, Germany

Abstract According to the hypothesis of aerosol invigoration, the higher concentration of aerosols in polluted air intensifies storms. A leading theory for explaining such a relationship is warm-phase invigoration, in which cloudy updrafts that are more polluted more readily condense water vapor onto liquid drops, thereby releasing latent heat faster, leading to higher buoyancies and higher updraft speeds. For this mechanism to work, water-vapor supersaturations well in excess of 1% must be typical of relatively unpolluted cloudy updrafts. Here, the supersaturation is calculated from in situ observations of warm-phase cloudy updrafts over the Amazon. Instead of values well in excess of 1%, the typical values are found to be around 0.2%. These observations imply that cleaner preindustrial air might have generated supersaturations around 1%, but those are still too low for warm-phase invigoration to have any practically significant impact on cloud buoyancy and updraft speeds.

Plain Language Summary An actively debated hypothesis is that air pollution from human activities regularly makes storms around the world more intense, with intensity measured, for example, by the speed of storm updrafts. There are three main proposed mechanisms for how aerosols might invigorate storms, one of which is the so-called "warm-phase invigoration mechanism." In this mechanism, extra particles of air pollution (aerosols) make storm updrafts more buoyant and, therefore, faster, with "warm-phase" referring to the lower altitudes where clouds are composed of liquid water (as opposed to ice). But this mechanism requires the water vapor in cloud updrafts to be far out of equilibrium, as measured by the supersaturation (the amount by which the relative humidity exceeds 100%). We show that observed supersaturations in storm clouds over the Amazon are much too low for this mechanism to operate. In other words, the warm-phase mechanism is unlikely to have any practically significant effect on storm intensity.

1. Introduction

Observations show that lightning flash rates and convective cloud top heights tend to be greater where aerosol concentrations are highest: flash rates are observed to be higher over marine shipping lanes (Thornton et al., 2017) and urban areas (Orville et al., 2001), and flash rates and the altitudes of high-reflectivity cloud are generally higher over land than the ocean (Zipser et al., 2006). Those relationships are not controversial, but it remains to be determined what causes them. A leading hypothesis, generally referred to as "aerosol invigoration," posits that higher aerosol concentrations cause higher cloud updraft speeds. But deep-convective updraft speeds are challenging to measure and it is difficult to prove that correlations between updrafts and aerosols are causal (instead of both being driven by synoptic conditions). As a result, the evidence for aerosol invigoration is sparse and indirect (Tao et al., 2012), and one of the most tantalizing pieces of evidence linking higher aerosol concentrations to lower cloud top temperatures (Li et al., 2011) was later shown to be statistically insignificant (Varble, 2018).

At least three different theories have been proposed for how high aerosol concentrations could increase cloud updraft speeds. One of those suggests that higher aerosol concentrations lead to greater lofting of liquid-water droplets to altitudes where they freeze, thereby releasing the latent heat of fusion, potentially increasing the updraft's buoyancy (Rosenfeld et al., 2008) if the lofted condensates can be unloaded fast enough (Grabowski & Morrison, 2016). Another theory suggests that higher aerosol concentrations lead to less precipitation and,
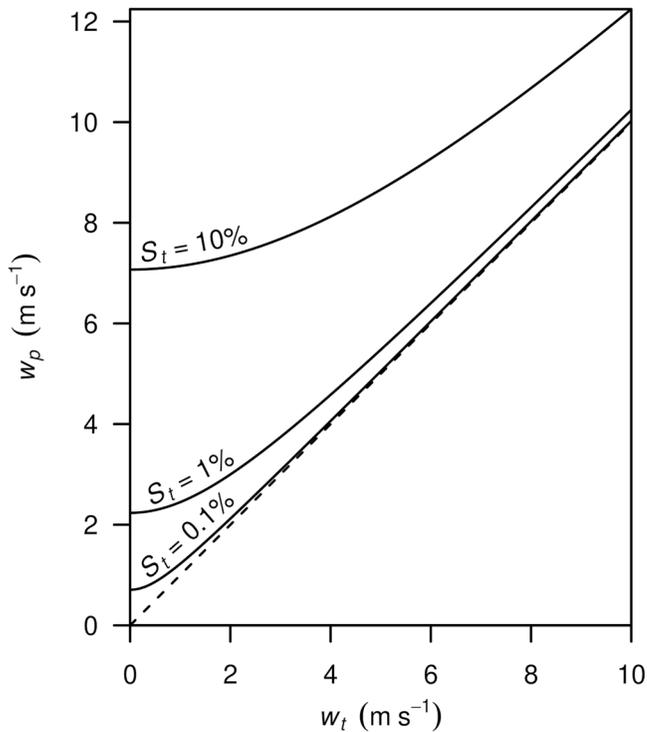
Figure 1. The velocity w_p of polluted updrafts from Equation 1 using $ar/c_d = 500$ m^2 s^{-2} plotted as a function of the velocity w_t of typical updrafts for three different values of the typical supersaturation S_t: 0.1%, 1%, and 10%. For visual reference, the dashed line marks $w_p = w_t$.

therefore, more detrainment moistening of the environment, which then, via convective entrainment, increases the buoyancy of subsequent updrafts (Abbott & Cronin, 2021). A third theory—and the focus of this study—is the so-called "warm-phase invigoration mechanism," which says that higher aerosol concentrations allow cloud updrafts to more readily condense water vapor onto liquid drops, thereby releasing latent heat sooner, enhancing the updrafts' buoyancy and vertical velocity (Fan et al., 2018; Saleeby et al., 2015; Sheffield et al., 2015).

Convective velocities are nearly invariant with respect to changes in atmospheric aerosols that are held constant in space and time because a moist convecting atmosphere adopts a state of marginal stability (i.e., nearly identical profiles of convective and environmental density) independent of microphysical details (Emanuel, 1994; Singh & O'Gorman, 2013). Accordingly, a large, sustained change to the aerosol number concentration induces only a negligible change to vertical velocities in radiative-convective equilibrium (Abbott & Cronin, 2021; van den Heever et al., 2011). Therefore, warm-phase invigoration is possible only if some updrafts are affected more than others. For example, if there were rare updrafts with especially high supersaturation, a uniform increase in pollution could warm those rare updrafts more than others, but this does not occur to any substantial degree in simulations (Abbott & Cronin, 2021; van den Heever et al., 2011). A more likely scenario is one in which an isolated plume of pollution warms the updrafts within it, thereby invigorating them. This scenario requires that typical updrafts have substantial supersaturation, and so we seek evidence of that in this study.

Let us denote typical and atypically polluted clouds by subscripts t and p, respectively. Here and throughout, "polluted" means polluted relative to the typical cloud updrafts, not polluted with respect to some absolute measure. Consider some height, which has a typical updraft vertical velocity w_t and typical updraft supersaturation S_t (equal to the relative humidity minus one). Due to its relatively high aerosol concentration, a polluted updraft will have, all else equal, a higher droplet number concentration and, therefore, S_p will be lower than S_t at that height. To give an upper bound on the invigoration, we can assume that S_p is so much smaller than S_t that it can be approximated as zero. We will henceforth refer to the difference $w_p - w_t$ obtained with $S_p = 0$ as the "potential invigoration."

All else equal (i.e., updrafts with the same size, cloud-base enthalpy, and fractional entrainment rate), the higher aerosol concentration in a polluted updraft does not affect its enthalpy, but it does cause relatively more of the enthalpy to take the form of sensible heat, thereby increasing the updraft's buoyancy. Assuming $S_p = 0$, the vertical velocity in a polluted updraft w_p is related to w_t and S_t by

$$w_p = \sqrt{w_t^2 + \frac{ar}{c_d} S_t}, \tag{1}$$

where r is the radius of the convective updraft, c_d is the drag coefficient for a cloudy updraft, and a takes a value around 1 m s^{-2} in the lower tropical troposphere (see Appendix A for a derivation). Numerical simulations (Hernandez-Deckers & Sherwood, 2016; Romps & Charn, 2015) and stereophotogrammetry (Romps & Öktem, 2015) indicate that a typical c_d is in the range of 0.2–1 and typical updraft radius is in the range of 200–1,000 m. Therefore, we will henceforth use $ar/c_d = 500$ m^2 s^{-2} in calculations of w_p.

Figure 1 plots w_p versus w_t for three different values of S_t: 10%, 1%, and 0.1%. We see that a typical in-cloud supersaturation of 10% allows for substantial potential invigoration. Later, we will see from observational data that updrafts have a typical lower-tropospheric updraft speed of 3 m s^{-1}, so we will focus on $w_t = 3$ m s^{-1} in our discussion here. We see from Figure 1 that, if typical updrafts have a supersaturation of 10% and a vertical velocity of 3 m s^{-1}, then the rare updraft that has an aerosol concentration much higher than typical could have a vertical velocity as high as 7.7 m s^{-1}. On the other hand, if the typical updrafts have a supersaturation of about 1%, then the potential invigoration of polluted updrafts is much more muted: a typical speed of 3 m s^{-1} could increase

to no more than 3.7 m s^{-1} in a polluted updraft. Finally, if the typical supersaturation is 0.1%, then the potential invigoration is negligible: a typical speed of 3 m s^{-1} would increase to more than 3.09 m s^{-1} in a polluted updraft. Therefore, a supersaturation of 1% serves as a dividing line between large potential invigoration (for $S_t \gg 1\%$) and negligible potential invigoration (for $S_t \ll 1\%$). This is consistent with previous work showing that $S_t - S_p = 20\%$ would give polluted updrafts a large virtual-temperature boost of ~1 K (Igel & van den Heever, 2021) while $S_t - S_p = 1\%$ would give polluted updrafts small, but possibly detectable, increases of ~0.1 K in virtual temperature (Grabowski & Jarecka, 2015) and ~0.5 m s^{-1} in updraft speed (Grabowski & Morrison, 2020). The question, then, is whether the typical supersaturation in warm-phase convecting clouds is closer to 10% or 0.1%.

The strongest evidence offered in favor of high supersaturation comes from a pair (labeled C_PI and C_BG) of cloud-resolving simulations (Fan et al., 2018) of convection over the Amazon during the Observations and Modeling of the Green Ocean Amazon (GoAmazon 2014/5) campaign (Martin et al., 2016), where the low aerosol concentrations favor higher supersaturation. In both a simulation with an aerosol number concentration representative of preindustrial conditions (130 cm^{-3}; C_PI) and a simulation with polluted conditions (950 cm^{-3}; C_BG), the mean profiles of warm-updraft supersaturation increased with height in the lower troposphere to well over 1%, reaching 15% and 6%, respectively (Fan et al., 2018).

Unfortunately, these high supersaturations cannot be confirmed with direct in situ measurements because the required accuracies for temperature and humidity are not achievable with current technology. The alternative is to calculate a proxy for supersaturation S—the quasi-steady-state supersaturation S_{QSS}—that can be calculated from measurements of the vertical velocity and drop size distribution (Squires, 1952) (see Text S5 in Supporting Information S1). Although this is the most reliable way to infer the supersaturation from observations, it has been used on only a handful of occasions (Politovich & Cooper, 1988; Prabha et al., 2011; Warner, 1968). Two of those studies (Politovich & Cooper, 1988; Warner, 1968) calculated supersaturations around 0.1%–0.2% while the other (Prabha et al., 2011) found supersaturations mainly below 1%, but with some values as high as ~10%.

Below, we will (a) confirm, using cloud-resolving simulations, that S_{QSS} closely replicates the actual S, and (b) use S_{QSS} to estimate S from in situ observations of updrafts during the contemporaneous GoAmazon and ACRIDION-CHUVA campaigns (Martin et al., 2016; Wendisch et al., 2016), chosen because these observations allow for a direct comparison with the polluted C_BG simulation that report high supersaturation (Fan et al., 2018). The observational results will also allow us to calculate the supersaturation to be expected in preindustrial conditions for comparison with C_PI.

2. Methods

A cloud's quasi-steady-state supersaturation S_{QSS} is defined to be the supersaturation S that would ensure a steady-state diffusion of water vapor onto the observed cloud drops given the observed vertical velocity. To the best of our knowledge, S_{QSS} has never been validated against the actual S in a cloud-resolving simulation with spectral-bin microphysics. To this end, we focus on a pair of simulations (C_PI and C_BG) designed and run by Fan et al. (2018) to represent meteorological conditions during the GoAmazon campaign on 17 March 2014 minus the plume of pollution from the nearby city of Manaus (see Text S1 in Supporting Information S1). In these simulations, we calculate S_{QSS} and the actual S within warm cloudy updrafts (WCU; defined as locations or grid cells with temperature >273 K, mass fraction >10^{-4} of droplets smaller than 100 micron in diameter, and vertical velocity >1 m s^{-1}). Defined in this way, WCU are responsible for the majority of latent heating in both simulations, so they are the "typical" convective elements responsible for setting the atmosphere's lapse rate. Since the observational data we will use comes from an aircraft that flew through the tops of convective clouds, we define warm cloudy updraft tops (WCUT) as the subset of WCU that are within a kilometer of the cloud top (with the "cloud top" for each column defined as the upper boundary of the highest grid cell with mass fraction of cloud liquid plus ice exceeding 10^{-4}). In the simulation results shown here, we sample the simulations from 0 to 1,000 m below cloud top, but the conclusions we reach are insensitive to that chosen altitude range (see Text S1 in Supporting Information S1 and associated figures). As we can see in Figure S1 of Supporting Information S1, WCUT grid points have a mean profile of supersaturation that grows with height to 6%–9% in the lower troposphere, qualitatively consistent with previous work (Fan et al., 2018).

Figure 2 shows the normalized distribution of WCUT volume from the WRF simulations on axes of log(S) (the abscissa) and log(S_{QSS}) (the ordinate); the distribution is normalized to give an integral of one over log(S)
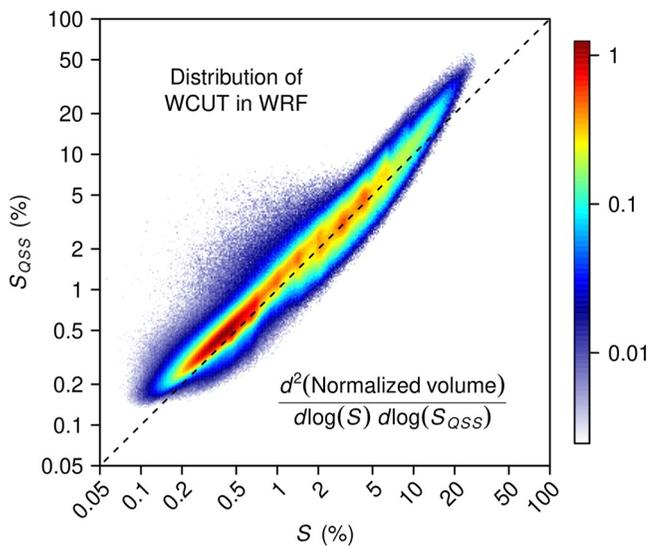
Figure 2. Normalized distribution of warm-cloudy-updraft-top volume within the cloud-resolving WRF simulations of GoAmazon convection. For visual reference, the dashed curve marks a one-to-one line. The logarithm of the quasi-steady-state supersaturation $\log(S_{QSS})$ is strongly correlated with the logarithm of the actual supersaturation $\log(S)$ ($r^2 = 0.92$) and, as a model for $\log(S)$, $\log(S_{QSS})$ explains 90% of the variance ($R^2 = 0.90$).

and $\log(S_{QSS})$. We see from Figure 2 that S_{QSS} is strongly correlated with S: the square of the Pearson correlation coefficient for $\log(S_{QSS})$ and $\log(S)$ is $r^2 = 0.92$. Note that the distribution is tightly clustered around the one-to-one line (Grabowski & Morrison, 2017). In fact, $\log(S_{QSS})$ by itself (i.e., without any further linear transformation) is a good model for $\log(S)$, explaining 90% of its variance (coefficient of determination $R^2 = 0.90$). Note from Figure 2 that S_{QSS} is biased slightly high relative to S. The bias is a relative amount of 20% in the geometric mean (i.e., $S = 1.0\%$ manifests as $S_{QSS} \approx 1.2\%$). This bias could be largely eliminated by incorporating ventilation factors for the hydrometeors in the calculation of S_{QSS}, but those expressions are uncertain. Therefore, we omit those ventilation factors and use the resulting S_{QSS}, with its slight high bias, as a direct proxy for S. Since we will be arguing that S is small in observations, this is a conservative choice.

To measure the supersaturation using the quasi-steady-state approximation in observed WCUT during the GoAmazon campaign, we use data collected during September 2014 aboard the High Altitude and Long Range Research Aircraft (HALO; see Text S2 in Supporting Information S1), which was flown through cloudy updrafts throughout the Amazon as part of the ACRIDICON-CHUVA campaign (Wendisch et al., 2016) in conjunction with GoAmazon. HALO flew through the tops of developing convective clouds at various heights and times (see Figure S2 in Supporting Information S1) and at locations that were outside of and far from the plume of pollution generated by the city of Manaus (see Figure S3 in Supporting Information S1).

As mentioned, the preindustrial (C_PI) and polluted (C_BG) simulations that reported high supersaturation (Fan et al., 2018) had aerosol number concentrations of $\sim$100 cm^{-3} and $\sim$1,000 cm^{-3}, respectively. The mean aerosol number concentration measured aboard HALO by the condensation particle counter (CPC; see Text S2 in Supporting Information S1) in clear air during the September flights below an altitude of 5 km above sea level and at least 100 km away from the Manaus airport was 1,400 cm^{-3}. On the three of those flight days identified as sampling "clean" air (September 11, 28, and 30) (Wendisch et al., 2016), this mean was 1,000 cm^{-3}, and all sampled WCUT were between 450 and 1,300 km away from Manaus. Likewise, the mean aerosol number concentration measured by a CPC in the boundary layer upwind of Manaus (see Text S3 in Supporting Information S1) during the September flights was 1,200 cm^{-3} overall and 1,100 cm^{-3} on the three "clean" days. Therefore, we can make an apples-to-apples comparison between data collected aboard HALO and the C_BG simulation, as both had an aerosol number concentration of $\sim$1,000 cm^{-3}. As discussed in Section 4, we can calculate how a preindustrial concentration of 100 cm^{-3} would have affected the supersaturation in the observed clouds, allowing us to compare to the supersaturation modeled in the C_PI simulation.

During the flights, the vertical wind speed was obtained from the Basic HALO Measurement and Sensor System (BAHAMAS). Two instruments were used to measure the distribution of cloud droplets: the Cloud and Aerosol Spectrometer (CAS; diameters of 0.89–50 micron) and the Cloud Droplet Probe (CDP; diameters of 2.5–46 micron) (Braga et al., 2017a, 2017b; Klingebiel et al., 2015; Molleker et al., 2014). Larger hydrometeors were measured with the Cloud Imaging Probe (CIP; diameters of 25–1,000 micron). Each instrument reported measurements at 1 Hz and the airplane flew through WCUT at a true airspeed ranging from 108 to 138 m s^{-1}, which makes each measurement a sample over $\sim$100 m. This spatial resolution is considerably finer than the 500-m grid spacing of the cloud-resolving simulations that report high supersaturation (Fan et al., 2018); all else equal, this should make fluctuations to high supersaturation even more frequently detected in the observations.

3. Results

Using CIP + CAS (CIP + CDP) aboard the HALO aircraft, and eliminating cases with incomplete data, there are 433 (461) observations of WCUT. Figure S4 in Supporting Information S1 shows the mean drop distribution in WCUT using CIP + CAS and CIP + CDP. The supersaturation is calculated using the quasi-steady-state approximation (see Text S5 in Supporting Information S1). The resulting 433 (461) supersaturation values are
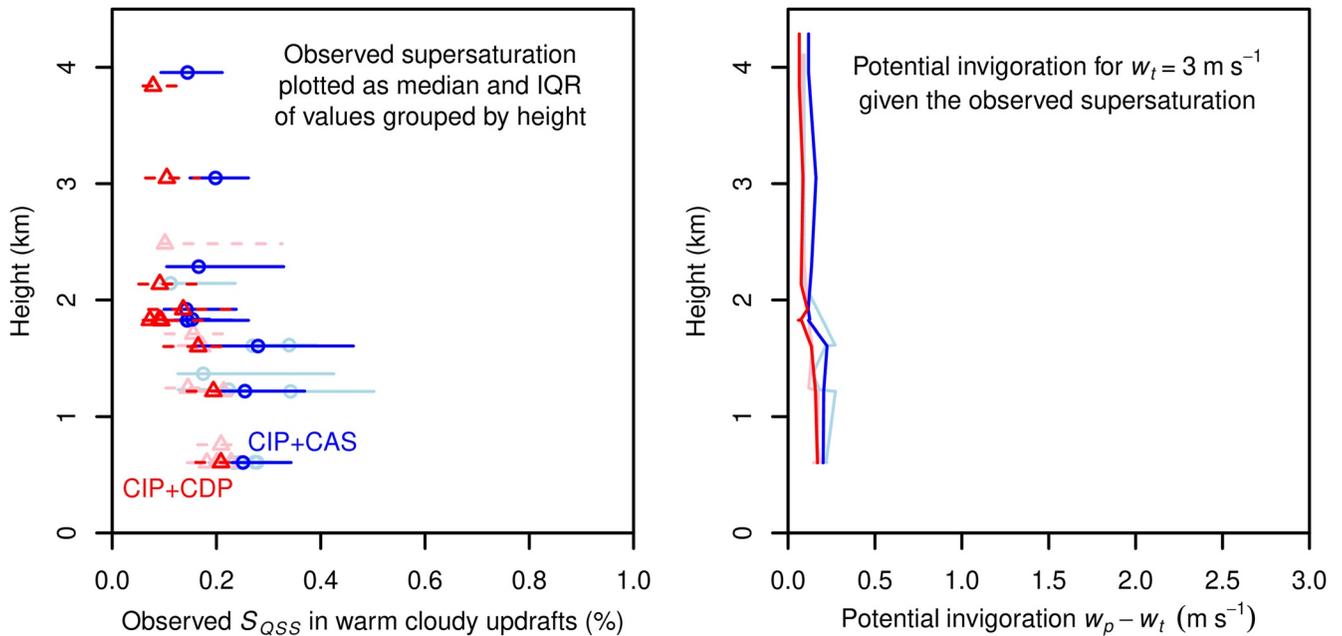
Figure 3. (left) The mean and interquartile range of supersaturation in each of 10 groups of measurements sorted by height above sea level for the (blue) CIP + CAS and (red) CIP + CDP pairings of instruments for all nine flight days in September. (right) Potential invigoration calculated using the mean values of supersaturation from those 10 groups and Equation 1 with $w_t = 3$ m s^{-1} and $ar/c_d = 500$ m^2 s^{-2}. (light blue and pink) Same, but for the three flight days deemed to be of air that was clean or marine.

grouped into 10 nearly equal-sized groups of 43 or 44 (46 or 47) values each, sorted by height. The means and interquartile ranges of each group are plotted at the group's mean height in blue and red in the left panel of Figure 3. These observed values of supersaturation differ markedly from the simulated values in two respects. First, the two sets of instruments (CIP + CAS and CIP + CDP) agree that the observed supersaturation in warm cloud updrafts averages about 0.2%, which is more than an order of magnitude smaller than in the simulations. Second, the observed profile of WCUT supersaturation decreases with height, contrary to the simulated increase with height. Plugging the observed mean profiles of supersaturation into Equation 1 for $w_t = 3$ m s^{-1}, we find that the potential invigoration, which is plotted in blue and red in the right panel of Figure 3, is only ~10–20 cm s^{-1}, which is negligible for all practical purposes. If this analysis is repeated for the 127 (144) supersaturation values measured on the three days (September 11, 28, and 30) when the sampled air was considered "clean" or "marine" (Wendisch et al., 2016), we get the results shown in light blue and pink in Figure 3, which tell the same story.

4. Discussion

The mean supersaturation of ~0.2% found here for warm-phase convective clouds over the Amazon is similar to the findings of ~0.1% supersaturation in cumuli over Australia (Warner, 1968) and ~0.2% supersaturation in cumuli over Montana (Politovich & Cooper, 1988). On the other hand, in situ measurements of warm-phase supersaturation as high as ~10% were reported from the CAIPEEX campaign over central India (Prabha et al., 2011), during which boundary-layer aerosol concentrations were ≳1,000 cm^{-3}. To understand the apparent discrepancy, we repeated the original analysis of those CAIPEEX data for all times when the airplane was in an updraft ($w > 1$ m s^{-1}; see Text S4 in Supporting Information S1). While this generates a handful of supersaturation values exceeding 5%, the mean is only 0.8%. Further restricting to warm cloudy updrafts, which requires that the updrafts be in warm-phase cloud with a cloud-liquid mass fraction exceeding 10^{-4}, the mean supersaturation becomes 0.3%, which is in line with the results found here (see Figures S5 and S6 in Supporting Information S1).

Although observations are broadly consistent in reporting mean supersaturations much less than 1%, the cloud-resolving simulation C_BG reported mean supersaturations much greater than 1%. In the quasi-steady-state approximation, which Figure 2 confirmed to be reasonable, the supersaturation is proportional to the vertical velocity divided by the "diameter concentration," that is, the sum of drop diameters per volume (see Text S5 in
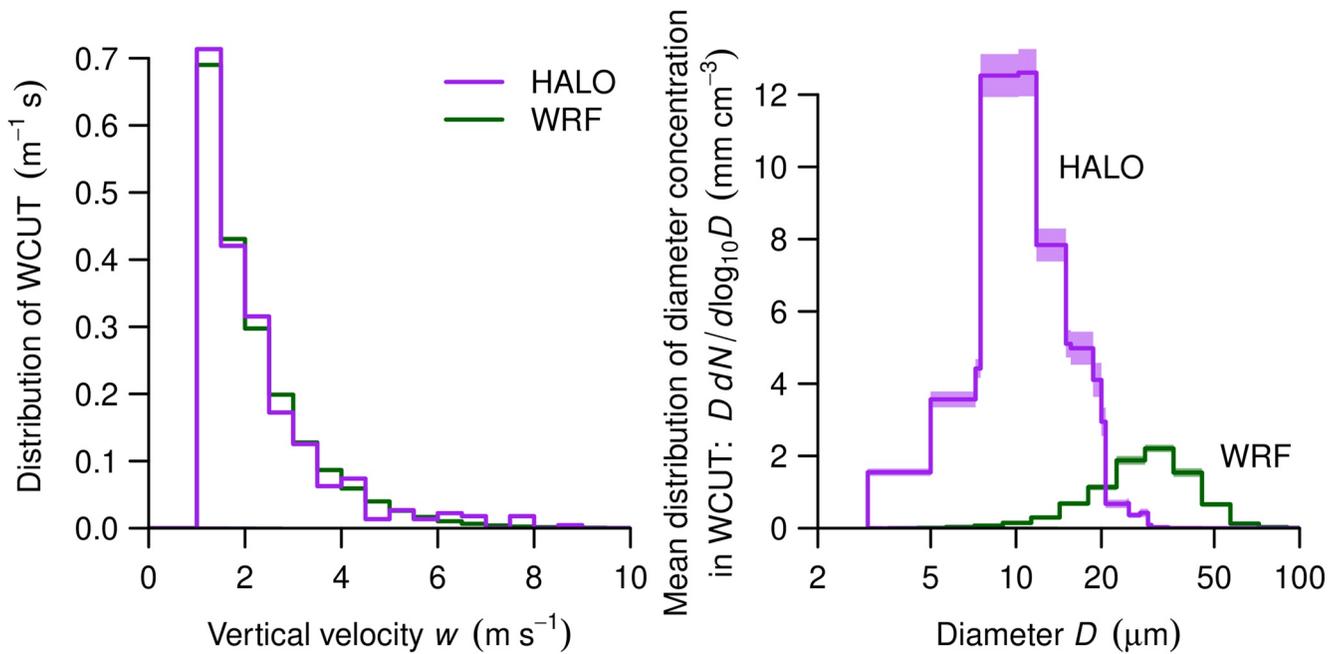
Figure 4. (left) Probability distributions of warm-cloudy-updraft-top (WCUT) vertical velocities from the C_BG WRF simulation and observations aboard HALO; the observed velocities are virtually identical to those in the simulations. (right) Mean normalized distribution of the sum of droplet diameter per volume, $D dN/d \log_{10}(D)$; simulated droplet spectra have larger droplets than observed, leading to a smaller sum of diameters (the area under the curve) and, therefore, higher supersaturation. In both panels, the HALO curves are of 1-Hz samples of WCUT and the WRF curves are the distributions of WCUT grid cells at each height that are then averaged together with weights equal to the number of 1-Hz HALO samples at those heights.

Supporting Information S1). Therefore, the observations and simulations must differ in one or both of the vertical velocity and diameter concentration. There is, however, no substantial difference in vertical velocity w. The left panel of Figure 4 plots the distributions of observed (HALO) and simulated (C_BG) WCUT vertical velocities. To ensure that we are comparing w values at the same heights, normalized distributions of WRF WCUT w are made at each height and then averaged together weighted by the number of HALO WCUT samples at those heights. The observed and simulated distributions have nearly identical means equal to 2.2 m s^{-1}.

Since the vertical velocities are the same, the simulation must have a very different diameter concentration. Indeed, this is corroborated by the right panel of Figure 4, which plots the contribution to the diameter concentration from drops of different diameters; here $N(D)$ is the number concentration of drops with diameters smaller than D. Again, to ensure an apples-to-apples comparison, WRF distributions at different heights are averaged together weighted by the number of HALO WCUT samples at those heights. We see that the simulation generates a diameter concentration (area under the curve) that is too small, caused by having drops that are too large and too few.

Both the C_BG simulation and the HALO observations had aerosol number concentrations around 1,000 cm^{-3}. To estimate the supersaturation to be expected in preindustrial conditions, that is, with aerosol concentrations of ∼100 cm^{-3} (Andreae, 2007), we will use two simplifying assumptions. The first assumption is that the cloud-droplet number concentration is proportional to the aerosol number concentration N; this ignores the negative feedback that supersaturation has on cloud-droplet number concentrations (a lower number concentration yields higher supersaturation, which activates additional cloud droplets, raising the number concentration). The second assumption is that the liquid-water mass fraction of the cloud is unaffected by N; this ignores the positive feedback that microphysics has on cloud-droplet number concentrations (a lower number concentration can increase collision, coalescence, and rainout, further reducing the number concentration). Any errors introduced by these assumptions tend to oppose one another. In combination, these two assumptions allow us to identify ND^3 as independent of N, where D is the characteristic droplet diameter, giving us $D \propto N^{-1/3}$. The quasi-steady-state supersaturation is proportional to the inverse of cloud-droplet number concentration times the mean droplet diameter (see Text S5 in Supporting Information S1), so the two simplifying assumptions give

$$S \propto \frac{1}{ND} \propto N^{-2/3}. \qquad (2)$$

In an atmosphere with $N \approx 1{,}000$ cm^{-3}, we have seen from observations that $S \approx 0.2\%$. Using Equation 2, we can estimate, therefore, that S for a preindustrial N of ~ 100 cm^{-3} would be $(100/1{,}000)^{-2/3} \times 0.2\% \approx 1\%$. This is at, but not exceeding, the threshold for practical relevance of warm-phase invigoration. This contrasts with the warm-phase supersaturation generated in the C_PI simulation, which had values of $\sim 15\%$, well in excess of the 1% threshold. Pushing Equation 2 even further, a warm-phase supersaturation of 10% would require $N = (1{,}000$ cm$^{-3}) \times (0.2/10)^{3/2} = 3$ cm^{-3}, which is at least an order of magnitude lower than typically observed over the remote oceans (Andreae, 2007). The absence of any potential warm-phase invigoration in polluted air ($S \approx 0.2\%$ for $N \approx 1{,}000$ cm^{-3}) and the inference of no substantial potential for warm-phase invigoration in preindustrial air ($S \approx 1\%$ for $N \approx 100$ cm^{-3}) suggest that warm-phase aerosol invigoration may be of no practical significance in Earth's atmosphere.

Throughout, we have assumed that atypically polluted updrafts have zero supersaturation, that is, $S_p = 0$. A more realistic assumption would be that supersaturation is reduced, but not zeroed, in polluted updrafts. For example, by Equation 2, a doubling of aerosol concentration would reduce the supersaturation by only 37%, yielding an invigoration well below the potential invigoration plotted in Figure 1. On the other hand, updrafts with $ar/c_d > 500$ m^2 s^{-2} will have a potential invigoration (even if not actual invigoration) larger than that plotted in Figure 1. And, although there is no evidence from simulations or observations that small pockets of high-supersaturation updrafts exist among updrafts that are otherwise low-supersaturation, their existence somewhere on Earth cannot be ruled out at this time.

Appendix A: Deriving w_p

The moist static energy $h(z)$ of an updraft is governed by $dh/dz = \varepsilon(h_e - h)$, where ε is the fractional entrainment rate and $h_e(z)$ is the moist static energy of environmental air. This implies that two updrafts with different aerosol concentrations (typical and polluted), but otherwise identical ε and initial h, will have the same enthalpy at a given height:

$$c_p T_t + L(1 + S_t)q_v^*(T_t) = c_p T_p + L(1 + S_p)q_v^*(T_p). \tag{A1}$$

Here, T_t and T_p are the temperatures of the typical and polluted updrafts, S_t and S_p are the supersaturations of the typical and polluted updrafts, $c_p = 1{,}005$ J kg^{-1} is the heat capacity of air at constant pressure, $L = 2.501 \times 10^6$ J kg^{-1} is the latent enthalpy of evaporation, and q_v^* is the saturation vapor mass fraction at the given pressure level. Using $S_p = 0$ to get the potential invigoration and using the Clausius-Clapeyron relation to approximate $q_v^*(T_p)$ as

$$q_v^*(T_p) \approx q_v^*(T_t) + \frac{Lq_v^*(T_t)}{R_v T^2}(T_p - T_t), \tag{A2}$$

where $R_v = 460.52$ J kg^{-1} K^{-1} is the specific gas constant of water vapor, we can rearrange Equation A1 as

$$\Delta T = \frac{Lq_v^*}{c_p + L^2 q_v^*/R_v T^2} S_t, \tag{A3}$$

where $\Delta T \equiv T_p - T_t$ is the difference in temperature between the polluted and typical plumes, and we have approximated $q_v^*(T_t)$ and T_t by the environmental values on the right-hand side. Writing the difference in buoyancy as $\Delta b = g\Delta T/T$, where $g = 9.81$ m s^{-2} is the gravitational acceleration, we get

$$\Delta b = \frac{gLq_v^*}{c_p T + L^2 q_v^*/R_v T} S_t. \tag{A4}$$

We can relate this to vertical velocity by noting that the momentum budget of updrafts can be approximated as a force balance between buoyancy and drag (Hernandez-Deckers & Sherwood, 2016; Romps & Charn, 2015),

$$b = \frac{3c_d}{8r} w^2, \tag{A5}$$

where r is the updraft's radius and c_d is an effective drag coefficient. This equation holds separately for the typical updrafts (with b_t and w_t) and for the polluted updrafts (with b_p and w_p); subtracting one of those equations from the other and solving for w_p yields

$$w_p = \sqrt{w_t^2 + \frac{8r}{3c_d}\Delta b}. \tag{A6}$$

Eliminating Δb using Equation A4, this gives

$$w_p = \sqrt{w_t^2 + \frac{ar}{c_d}S_t}, \tag{A7}$$

where

$$a \equiv \frac{8g}{3}\frac{Lq_v^*}{c_pT + L^2q_v^*/R_vT}. \tag{A8}$$

The value of a varies from about 1.1 m s^{-2} in tropical surface air to about 0.8 m s^{-2} at the tropical melting line.

Data Availability Statement

The cloud-resolving model data are available at https://data.pnnl.gov/group/nodes/dataset/13425. The boundary-layer aerosol number concentrations upwind of Manaus are available at http://ftp.lfa.if.usp.br/ftp/public/LFA_Processed_Data/T0a_ATTO/Level1. The data collected aboard HALO during ACRIDICON-CHUVA are available at https://halo-db.pa.op.dlr.de/mission/5.

References

Abbott, T. H., & Cronin, T. W. (2021). Aerosol invigoration of atmospheric convection through increases in humidity. *Science*, *371*(6524), 83–85. https://doi.org/10.1126/science.abc5181

Andreae, M. O. (2007). Aerosols before pollution. *Science*, *315*(5808), 50–51. https://doi.org/10.1126/science.1136529

Braga, R. C., Rosenfeld, D., Weigel, R., Jurkat, T., Andreae, M. O., Wendisch, M., et al. (2017a). Comparing parameterized versus measured microphysical properties of tropical convective cloud bases during the ACRIDICON-CHUVA campaign. *Atmospheric Chemistry and Physics*, *17*(12), 7365–7386. https://doi.org/10.5194/acp-17-7365-2017

Braga, R. C., Rosenfeld, D., Weigel, R., Jurkat, T., Andreae, M. O., Wendisch, M., et al. (2017b). Further evidence for CCN aerosol concentrations determining the height of warm rain and ice initiation in convective clouds over the Amazon basin. *Atmospheric Chemistry and Physics*, *17*(23), 14433–14456. https://doi.org/10.5194/acp-17-14433-2017

Emanuel, K. A. (1994). *Atmospheric convection*. Oxford University Press.

Fan, J., Rosenfeld, D., Zhang, Y., Giangrande, S. E., Li, Z., Machado, L. A. T., et al. (2018). Substantial convection and precipitation enhancements by ultrafine aerosol particles. *Science*, *359*(6374), 411–418. https://doi.org/10.1126/science.aan8461

Grabowski, W. W., & Jarecka, D. (2015). Modeling condensation in shallow nonprecipitating convection. *Journal of the Atmospheric Sciences*, *72*(12), 4661–4679. https://doi.org/10.1175/jas-d-15-0091.1

Grabowski, W. W., & Morrison, H. (2016). Untangling microphysical impacts on deep convection applying a novel modeling methodology. Part II: Double-moment microphysics. *Journal of the Atmospheric Sciences*, *73*(9), 3749–3770. https://doi.org/10.1175/jas-d-15-0367.1

Grabowski, W. W., & Morrison, H. (2017). Modeling condensation in deep convection. *Journal of the Atmospheric Sciences*, *74*(7), 2247–2267. https://doi.org/10.1175/jas-d-16-0255.1

Grabowski, W. W., & Morrison, H. (2020). Do ultrafine cloud condensation nuclei invigorate deep convection? *Journal of the Atmospheric Sciences*, *77*(7), 2567–2583. https://doi.org/10.1175/jas-d-20-0012.1

Hernandez-Deckers, D., & Sherwood, S. C. (2016). A numerical investigation of cumulus thermals. *Journal of the Atmospheric Sciences*, *73*(10), 4117–4136. https://doi.org/10.1175/jas-d-15-0385.1

Igel, A. L., & van den Heever, S. C. (2021). Invigoration or enervation of convective clouds by aerosols? *Geophysical Research Letters*, *48*(16), e2021GL093804. https://doi.org/10.1029/2021gl093804

Klingebiel, M., de Lozar, A., Molleker, S., Weigel, R., Roth, A., Schmidt, L., et al. (2015). Arctic low-level boundary layer clouds: In situ measurements and simulations of mono-and bimodal supercooled droplet size distributions at the top layer of liquid phase clouds. *Atmospheric Chemistry and Physics*, *15*(2), 617–631. https://doi.org/10.5194/acp-15-617-2015

Li, Z., Niu, F., Fan, J., Liu, Y., Rosenfeld, D., & Ding, Y. (2011). Long-term impacts of aerosols on the vertical development of clouds and precipitation. *Nature Geoscience*, *4*(12), 888–894. https://doi.org/10.1038/ngeo1313

Martin, S. T., Artaxo, P., Machado, L. A. T., Manzi, A. O., Souza, R. A. F., Schumacher, C., et al. (2016). Introduction: Observations and modeling of the Green Ocean Amazon (GoAmazon2014/5). *Atmospheric Chemistry and Physics*, *16*(8), 4785–4797. https://doi.org/10.5194/acp-16-4785-2016

Molleker, S., Borrmann, S., Schlager, H., Luo, B., Frey, W., Klingebiel, M., et al. (2014). Microphysical properties of synoptic-scale polar stratospheric clouds: In situ measurements of unexpectedly large HNO$_3$-containing particles in the Arctic vortex. *Atmospheric Chemistry and Physics*, *14*(19), 10785–10801. https://doi.org/10.5194/acp-14-10785-2014

Orville, R. E., Huffines, G., Nielsen-Gammon, J., Zhang, R., Ely, B., Steiger, S., et al. (2001). Enhancement of cloud-to-ground lightning over Houston, Texas. *Geophysical Research Letters*, *28*(13), 2597–2600. https://doi.org/10.1029/2001gl012990

Politovich, M. K., & Cooper, W. A. (1988). Variability of the supersaturation in cumulus clouds. *Journal of the Atmospheric Sciences*, *45*(11), 1651–1664. https://doi.org/10.1175/1520-0469(1988)045<1651:votsic>2.0.co;2

Prabha, T. V., Khain, A., Maheshkumar, R. S., Pandithurai, G., Kulkarni, J. R., Konwar, M., & Goswami, B. N. (2011). Microphysics of premonsoon and monsoon clouds as seen from in situ measurements during the Cloud Aerosol Interaction and Precipitation Enhancement Experiment (CAIPEEX). *Journal of the Atmospheric Sciences*, *68*(9), 1882–1901. https://doi.org/10.1175/2011jas3707.1

Romps, D. M., & Charn, A. B. (2015). Sticky thermals: Evidence for a dominant balance between buoyancy and drag in cloud updrafts. *Journal of the Atmospheric Sciences*, *72*(8), 2890–2901. https://doi.org/10.1175/jas-d-15-0042.1

Romps, D. M., & Öktem, R. (2015). Stereo photogrammetry reveals substantial drag on cloud thermals. *Geophysical Research Letters*, *42*(12), 5051–5057. https://doi.org/10.1002/2015gl064009

Rosenfeld, D., Lohmann, U., Raga, G. B., O'Dowd, C. D., Kulmala, M., Fuzzi, S., et al. (2008). Flood or drought: How do aerosols affect precipitation? *Science*, *321*(5894), 1309–1313. https://doi.org/10.1126/science.1160606

Saleeby, S. M., Herbener, S. R., van den Heever, S. C., & L'Ecuyer, T. (2015). Impacts of cloud droplet–nucleating aerosols on shallow tropical convection. *Journal of the Atmospheric Sciences*, *72*(4), 1369–1385. https://doi.org/10.1175/jas-d-14-0153.1

Sheffield, A. M., Saleeby, S. M., & van den Heever, S. C. (2015). Aerosol-induced mechanisms for cumulus congestus growth. *Journal of Geophysical Research: Atmospheres*, *120*(17), 8941–8952. https://doi.org/10.1002/2015jd023743

Singh, M. S., & O'Gorman, P. A. (2013). Influence of entrainment on the thermal stratification in simulations of radiative-convective equilibrium. *Geophysical Research Letters*, *40*(16), 4398–4403. https://doi.org/10.1002/grl.50796

Squires, P. (1952). The growth of cloud drops by condensation. I. General characteristics. *Australian Journal of Chemistry*, *5*(1), 59–86. https://doi.org/10.1071/ch9520059

Tao, W.-K., Chen, J.-P., Li, Z., Wang, C., & Zhang, C. (2012). Impact of aerosols on convective clouds and precipitation. *Reviews of Geophysics*, *50*(2), RG2001. https://doi.org/10.1029/2011rg000369

Thornton, J. A., Virts, K. S., Holzworth, R. H., & Mitchell, T. P. (2017). Lightning enhancement over major oceanic shipping lanes. *Geophysical Research Letters*, *44*(17), 9102–9111. https://doi.org/10.1002/2017gl074982

van den Heever, S. C., Stephens, G. L., & Wood, N. B. (2011). Aerosol indirect effects on tropical convection characteristics under conditions of radiative-convective equilibrium. *Journal of the Atmospheric Sciences*, *68*(4), 699–718. https://doi.org/10.1175/2010jas3603.1

Varble, A. (2018). Erroneous attribution of deep convective invigoration to aerosol concentration. *Journal of the Atmospheric Sciences*, *75*(4), 1351–1368. https://doi.org/10.1175/jas-d-17-0217.1

Warner, J. (1968). The supersaturation in natural clouds. *Journal de Recherches Atmospheriques*, *3*(3), 233–237.

Wendisch, M., Pöschl, U., Andreae, M. O., Machado, L. A., Albrecht, R., Schlager, H., et al. (2016). ACRIDICON–CHUVA campaign: Studying tropical deep convective clouds and precipitation over Amazonia using the new German research aircraft HALO. *Bulletin of the American Meteorological Society*, *97*(10), 1885–1908. https://doi.org/10.1175/bams-d-14-00255.1

Zipser, E. J., Cecil, D. J., Liu, C., Nesbitt, S. W., & Yorty, D. P. (2006). Where are the most intense thunderstorms on Earth? *Bulletin of the American Meteorological Society*, *87*(8), 1057–1071. https://doi.org/10.1175/bams-87-8-1057

References From the Supporting Information

Andreae, M. O., Acevedo, O. C., Araùjo, A., Artaxo, P., Barbosa, C. G. G., Barbosa, H. M. J., et al. (2015). The Amazon Tall Tower Observatory (ATTO): Overview of pilot measurements on ecosystem ecology, meteorology, trace gases, and aerosols. *Atmospheric Chemistry and Physics*, *15*(18), 10723–10776. https://doi.org/10.5194/acp-15-10723-2015

Fan, J., Leung, L. R., Li, Z., Morrison, H., Chen, H., Zhou, Y., et al. (2012). Aerosol impacts on clouds and precipitation in eastern China: Results from bin and bulk microphysics. *Journal of Geophysical Research*, *117*(D16). https://doi.org/10.1029/2011jd016537

Fukuta, N., & Walter, L. A. (1970). Kinetics of hydrometeor growth from a vapor-spherical model. *Journal of the Atmospheric Sciences*, *27*(8), 1160–1172. https://doi.org/10.1175/1520-0469(1970)027<1160:kohgfa>2.0.co;2

Khain, A., Pokrovsky, A., Pinsky, M., Seifert, A., & Phillips, V. (2004). Simulation of effects of atmospheric aerosols on deep turbulent convective clouds using a spectral microphysics mixed-phase cumulus cloud model. Part I: Model description and possible applications. *Journal of the Atmospheric Sciences*, *61*(24), 2963–2982. https://doi.org/10.1175/jas-3350.1

Mei, F., Wang, J., Comstock, J. M., Weigel, R., Krämer, M., Mahnke, C., et al. (2020). Comparison of aircraft measurements during GoAmazon2014/5 and ACRIDICON-CHUVA. *Atmospheric Measurement Techniques*, *13*(2), 661–684. https://doi.org/10.5194/amt-13-661-2020

Paluch, I. R., & Knight, C. A. (1984). Mixing and the evolution of cloud droplet size spectra in a vigorous continental cumulus. *Journal of the Atmospheric Sciences*, *41*(11), 1801–1815. https://doi.org/10.1175/1520-0469(1984)041<1801:mateoc>2.0.co;2

Rogers, R. R., & Yau, M. K. (1989). *A short course in cloud physics* (3rd ed.). Butterworth-Heinemann.

Romps, D. M. (2014). An analytical model for tropical relative humidity. *Journal of Climate*, *27*(19), 7432–7449. https://doi.org/10.1175/jcli-d-14-00255.1

Romps, D. M. (2017). Exact expression for the lifting condensation level. *Journal of the Atmospheric Sciences*, *74*(12), 3891–3900. https://doi.org/10.1175/jas-d-17-0102.1

Romps, D. M. (2021). The Rankine-Kirchhoff approximations for moist thermodynamics. *Quarterly Journal of the Royal Meteorological Society*, *147*(740), 3493–3497. https://doi.org/10.1002/qj.4154

Skamarock, W. C., Klemp, J. B., Dudhia, K., Gill, D. O., Barker, D. M., Duda, M. G., et al. (2008). *A description of the advanced research WRF version 3 (NCAR Technical Note Nos. NCAR/TN-475+STR)*. National Center for Atmospheric Research.

Weigel, R., Spichtinger, P., Mahnke, C., Klingebiel, M., Afchine, A., Petzold, A., et al. (2016). Thermodynamic correction of particle concentrations measured by underwing probes on fast-flying aircraft. *Atmospheric Measurement Techniques*, *9*(10), 5135–5162. https://doi.org/10.5194/amt-9-5135-2016

Erratum

The originally published version of this article contained errors. In the captions of Figures 1 and 3, in the last sentence of the fifth paragraph of the Introduction, and in the fourth sentence of the last paragraph of Section 4, "1,000 m^2 s^{-2}" should read "500 m^2 s^{-2}." In the caption of Figure 1 and in the last sentence of the fifth paragraph of the Introduction, the expression "a/rc_d" should read "ar/c_d." These errors have been corrected, and this may be considered the authoritative version of record.